Journal of Geodesy (2024) 98:8
https://doi.org/10.1007/s00190-023-01814-1

ORIGINAL ARTICLE

The miniSLR: a low-budget, high-performance satellite laser ranging ground station

Daniel Hampf[1,2] · Felicitas Niebler[1] · Tristan Meyer[1] · Wolfgang Riede[1]

Received: 23 June 2023 / Accepted: 2 December 2023

Abstract
Satellite Laser Ranging (SLR) is an established technique providing very accurate position measurements of satellites in Earth orbit. However, despite decades of development, it remains a complex and expensive technology, which impedes its further growth to new applications and users. The miniSLR implements a complete SLR system within a small, transportable enclosure. Through this design, costs of ownership can be reduced significantly, and the process of establishing a new SLR site is greatly simplified. A number of novel technical solutions have been implemented to achieve a good laser ranging performance despite the small size and simplified design. Data from the initial six months of test operation have been used to generate a first estimation of the system performance. The data include measurements to many of the important SLR satellites, such as Lageos, Etalon and most of the geodetic and Earth observation missions in LEO. It is shown that the miniSLR achieves sub-centimetre accuracy, comparable with conventional SLR systems. The miniSLR is an engineering station in the International Laser Ranging Service and supplies data to the community. Continuous efforts are undertaken to further improve the system operation and stability.

Keywords Satellite laser ranging · Satellite geodesy · Ground stations · New space

1 Introduction

Satellite Laser Ranging (SLR) is a powerful tool for geodesy, mission support and fundamental science (Pearlman et al. 2019). However, the effort to construct and operate an SLR ground station is considerable and poses an entry barrier for new users and applications. Thus, the existing SLR network (see International Laser Ranging Service, ILRS (2023), Pearlman et al. (2019)), still suffers from significant gaps in global coverage, especially in the Global South.

Simulation studies (Otsubo et al. 2016; Glaser et al. 2019; Kehm et al. 2019) have shown that more SLR ground stations can significantly improve the terrestrial reference frame. Depending on performance assumptions, single stations can improve geocentre, scale and the Earth rotation parameters by 1–7%. However, while some terms would benefit most from a new SLR station near the South Pole, others would improve rather by additional stations near the equator, in the Arctic, and regions of the Pacific and Indian Ocean (Kehm et al. 2019). The effects are partly cumulative, and adding 14 additional stations has been found to improve geocentre and scale by around 20% (Glaser et al. 2019).

Apart from the improvement of geodetic parameters, new SLR stations are also in high demand for other applications: An increasing number of high-precision Earth observation missions requires SLR support, as well as the new generations of Global Navigation Satellite Systems. Recent years have seen a steady increase of SLR missions, with 120 targets currently officially supported by the ILRS (2023). In the future, SLR may also be used for space situational awareness, precise orbit determination and conjunction assessment, further increasing demand of ground stations (Hampf et al. 2021).

Already today demand can only be met with a tight schedule and in favourable weather conditions. More stations may be needed in the future to satisfy all ranging requirements. Furthermore, some older stations reach the end of their lifetime and will need replacement in coming years (Wilkinson et al. 2019).

✉ Daniel Hampf
daniel.hampf@digos.eu

[1] Institute of Technical Physics, German Aerospace Center, Pfaffenwaldring 38-40, 70569 Stuttgart, BW, Germany

[2] DiGOS Potsdam GmbH, Telegrafenberg, 14473 Potsdam, BB, Germany

Published online: 29 January 2024

Table 1 ILRS station parameters

System name	miniSLR
4-character code	SMIL
CDP system number	52
CDP Occupation Number	02
IERS DOMES number	10916S001
CDP Pad ID	7816
Location	Stuttgart, Germany
Latitude	48.74889398° N
Longitude	9.10259952° E
Elevation	533.240 m

The coordinates are approximate, based on a GNSS survey

On the other hand, technical advances of the last twenty years have opened the possibility to construct much smaller, simpler and cheaper SLR ground stations. Compact and powerful lasers, better detectors, faster readout electronics and PCs, and inexpensive but precise direct drive telescope mounts are key technologies for this development. The goal of the miniSLR project has been to combine these novel technologies for the first time into a working prototype of a new generation of SLR ground station. At a fraction of the cost of a conventional SLR system, it is designed to reach the same performance in terms of precision, stability and tracking capabilities.

A first version of the miniSLR has been constructed and set up at the DLR (German Aerospace Center) in Stuttgart. In its current configuration, it commenced experimental operation in November 2022. It has been accepted into the ILRS as engineering station, and data from measured passes have been uploaded to the European Data Center (EDC 2023). Table 1 lists the station's ILRS IDs and coordinates.

This paper describes the technical design (Sect. 2) and results from the first six months of test operation (Sect. 3). In the final Sect. 4, an outlook to the next steps in development and to the potential impact of this new development for the SLR and space geodesy community is given.

2 System set-up

2.1 Design innovations

This section highlights the main design features of the miniSLR that enable the reduction of size and complexity of the system. A full system overview is given in subsequent Sect. 2.2.

Fig. 1 The miniSLR prototype on the roof of the DLR institute building. The enclosure in the bottom contains most of the electronics and IT. The top compartments house the receive and transmit telescopes, the laser head, cameras, detectors and beam control optics

2.1.1 Transportability and small overall size

The main design goal of the miniSLR has been a significant reduction in the size of the system. Using a receive telescope of only 20 cm aperture and a small direct drive astronomy mount, the whole system could be integrated within and on top of an aluminium enclosure with a footprint of 130 x 230 cm (see Fig. 1). At a weight of about 600 kg, the enclosure can be moved around on wheels and installed for operation on any flat and stable surface.

The main advantages of this integrated design are:

- Lower production cost
- Lower maintenance cost
- The system can be integrated and validated at factory, before it is moved to its operation site, thus lowering the effort for installation and decreasing delays in the commissioning process.

- No need for civil engineering, building permits and construction works, thus significantly lowering costs, effort and time needed for installation.
- Re-location can be achieved easily, if necessary.

Some of these advantages have already been demonstrated by the French Transportable Laser Ranging Station (FTLRS, Nicolas et al. (2001)).

2.1.2 Fully sealed, no dome

The miniSLR system is fully sealed, thus avoiding the need for a dome with movable parts. This offers two main advantages: First, in case of a catastrophic failure (e.g. complete power loss, mechanical blockage etc.), the system remains in an inherently safe status (i.e. protected from rain). Recovery and repair can be planned and conducted with much less urgency than in the case of a dome that can no longer be closed. Second, the whole system is air-conditioned and retains a constant temperature in all parts. Combined with the relatively short cable lengths, this increases the stability of the timing measurement.

2.1.3 High repetition rate Q-switch laser

Due to the small aperture of the receive telescope, a rather high power laser is needed to achieve sufficient returns. On the other hand, relatively stringent size and weight limitations apply, since the laser head must be mounted in the top compartment. This was resolved by using high-repetition laser ranging (Hampf et al. 2019) with a small Q-switched diode laser. In this context, it offers three advantages:

- Sufficient average power at a very small footprint: At a size of 12 cm x 8 cm x 4 cm, the laser offers a power of 4.2 Watts (85 µJ at 50 kHz).
- Due to the low pulse energy, single photon operation is inherently ensured (at the given aperture and divergence). Avoiding additional attenuation components further simplifies the design.
- The high repetition rate results in a high number of returns for most targets, which decreases the statistical error of the average data points. This enables sufficiently precise measurements despite the relatively long pulse duration of 500 ps (FWHM).

2.1.4 Laser ranging at 1064 nm (near-infrared)

Using the Nd:YAG fundamental wavelength of 1064 nm for laser ranging has been discussed for many years (e.g. Völker et al. (2013)) and has recently been implemented in a number of SLR systems (Courde et al. (2017), Xue et al. (2016), Eckl et al. (2017), IZN-1 at Teneriffa). Nevertheless, most systems still use frequency doubling to obtain green laser light at 532 nm. This choice is primarily due to the available receive detectors: Up until a few years ago, single photon detectors with picosecond timing precision have only been realized for the visible light spectrum (either photomultiplier tubes or silicon-based geiger mode avalanche photo diodes). Today, however, InGaAs SPADs (single photon avalanche diodes based on indium gallium arsenide) achieve sufficient timing precision and good sensitivity at 1064 nm. With these, ranging at the fundamental Nd:YAG wavelength becomes more favourable for a number of reasons:

- Avoiding conversion losses, thus generating up to four times more photons from the same laser power (important to keep laser size and weight small)
- Avoiding complexity of additional frequency doubling optics
- Slightly better atmospheric transmission
- Less noise from sky brightness, especially at daylight (blue sky)

However, using 1064 nm instead of 532 nm also increases the diffraction-limited divergence of the laser beam by a factor of two and thus decreases the number of photons on the target by a factor of four (see also Sects. 2.2.2 and 2.4.3). This could be mitigated by using a larger beam exit aperture, which may be considered for a future version of the system.

2.2 Hardware set-up

This section gives a brief overview of the hardware set-up of the miniSLR. References to "item NN" relate to the indicators in Figs. 2 and 3.

2.2.1 Tracking and mechanics

Tracking is realized using an Astelco NTM-600 direct drive mount. It allows programming of custom trajectories, which are followed with a high timing precision owing to an internal GNSS clock. Thus, sufficiently accurate tracking to satellites with good predictions can be achieved. For simplicity, the pointing model is done by the main control software (see Sect. 2.3) rather than the mount's own firmware. For rain protection, the mount is wrapped in a Telegizmos telescope cover.

The optical set-up, including receive and transmit telescopes, is mounted on three optical breadboards installed on top of the mount. This enables a high degree of flexibility in the optical configuration, which is of paramount importance for an experimental prototype.

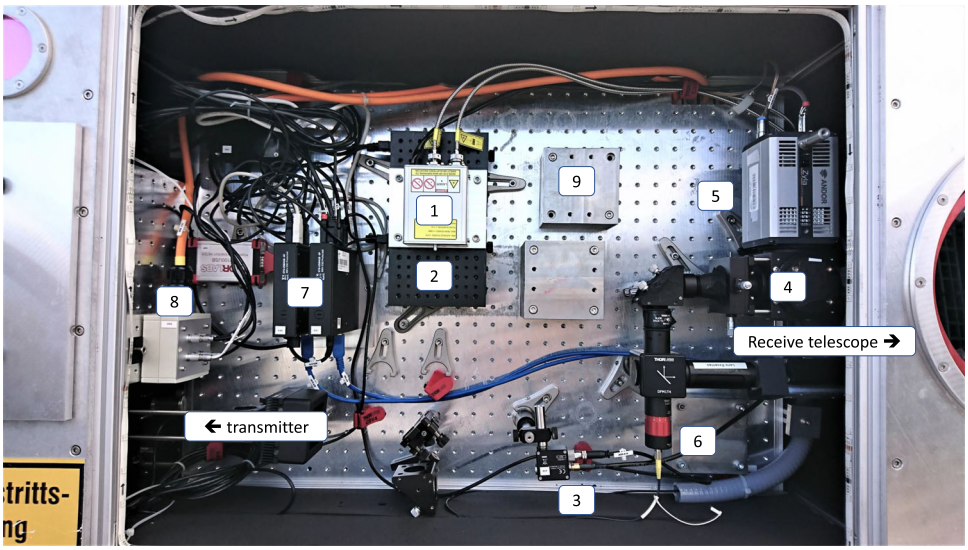

Fig. 2 The central compartment of the miniSLR head: (1) laser head; (2) thermo-electric elements (TEC) for laser temperature control; (3) start photodiode; (4) dichroic beam splitter; (5) tracking camera; (6) fibre coupling for single photon detector; (7) programmable USB hubs; (8) 12 V power distribution; (9) counter weights to balance mount elevation axis

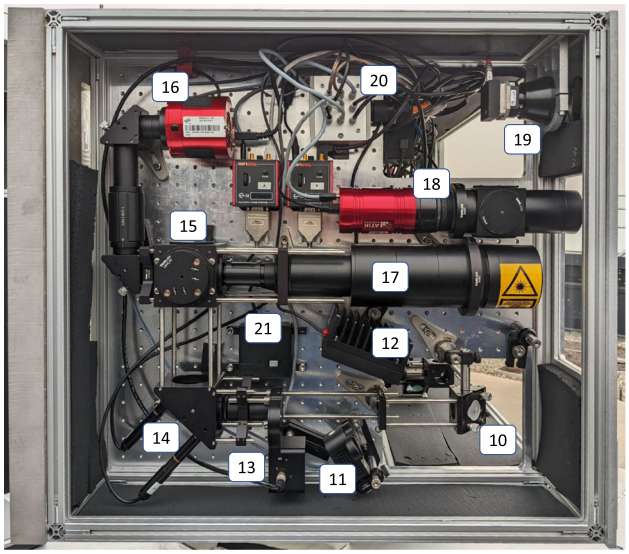

Fig. 3 The transmitter compartment of the miniSLR head: (10) incoming beam from central compartment; (11) attenuator flip mirror; (12) laser power meter; (13) safety shutter; (14) motorized beam steering mirror; (15) dichroic mirror guiding 1064 nm towards exit aperture; (16) transmitter camera; (17) beam expander; (18) backscatter camera; (19) aircraft camera; (20) power distribution; (21) thermometer/hygrometer

2.2.2 Transmit path

Laser pulses are produced by a Standa MOPA-4 diode laser (item 1). Its specifications are ideally suited for a small SLR system: The tiny laser head can easily be installed on the moving platform. A pulse duration of 500 ps FWHM is sufficiently short to achieve a high precision in averaged normal point data (see Sects. 2.4.1 and 2.4.2 for a more detailed discussion on ranging precision). A pulse energy of 85 µJ is enough to achieve returns from all relevant satellites, and a repetition rate of 50 kHz provides a high amount of data points for effective averaging (see also Sect. 2.4.3).

Temperature control for the laser head is realized by two Thorlabs PTC1/M thermoelectric elements. They keep the laser head at constant 22° Celsius and can dissipate up to 35 W of heat (item 2).

Pulse emission times are recorded with a standard photodiode (Thorlabs DET08C/M) using a fraction of light leaking through the first mirror (item 3). From the mirror, the light is guided towards the transmitter compartment (item 10).

For calibration, laser power needs to be strongly attenuated in order to not saturate the detector. This is achieved by a flip mirror carrying a reflective neutral density or laser line filter (item 11). It is closed by default and only opens when the system is tracking a satellite. While closed, the laser power is directed into a power meter (item 12). The laser average power is thus monitored and recorded each time a calibration run is performed. The subsequent safety shutter (item 13) is also closed by default and opens only for ranging measurements. It is spring-loaded and requires a regular "open" signal from the software to open and remain open (for more information on the safety system, see also Sect. 2.2.5).

The motorized beam mirror (item 14) is needed to fine-control the laser beam direction in relation to the main system pointing. It is moved by two Thorlabs Z806 motors, controlled by the main software.

The dichroic mirror (item 15) guides the infrared laser light towards the exit aperture, while incoming light passes through to the transmitter camera (item 16). This camera records the field of view seen by the beam expander and can be used during the initial alignment of the system. The beam expander itself (item 17) is a simple Galileo type telescope with a one-inch negative and a three-inch positive lens. It increases the beam diameter by about a factor of five, thus

Table 2 Main specifications of the miniSLR optical system

Transmit aperture	7.5 cm	
Beam diameter	5 cm	
Receive aperture (nominal)	20 cm	
Obscuration	25%	Due to secondary mirror in telescope
Laser pulse energy	85 µJ	(Measured)
Laser repetition rate	50 kHz	(Measured)
Operating wavelength	1064 nm	
Beam divergence	50 µrad	(Half angle, estimated)
Beam stability	50 µrad	(Half angle, estimated)
Transmitter efficiency	0.6	(Measured)
Receiver efficiency	0.1	(Estimated, losses e.g. in band-pass filter)
Efficiency of detector	30%	(Given by manufacturer)

These values are also used for calculation of the expected return rates (Sect. 2.4.3)

decreasing the beam divergence and improving the beam pointing resolution.

The backscatter camera (item 18) is used to monitor the laser beam in the atmosphere and fine-align it towards the target.

2.2.3 Receive path

The receive path starts with a 20 cm aperture Newton telescope (ASA H8). While a Newton telescope causes more issues with optical alignment than other telescope types, it features a favourably short mechanical length for a given aperture. A dichroic mirror on its exit port (item 4) guides visible light towards the main tracking camera (item 5), while transmitting the returning infrared laser light towards the single photon receiver. Two bandpass filters block light from 900 nm to 1700 nm, with a 1 nm wide window at 1064 nm. While not really required at night, these filters are essential for daylight ranging. For simplicity, they are permanently installed and not removed for night time ranging.

The light is coupled into a 105 µm multimode optical fibre connected to an Aurea SPD-OEM-NIR single photon detector, which generates the stop signal for the ranging measurement. The chosen combination of fibre and coupler exhibit a flat acceptance curve for light up to 15 arcsec from the optical axis. Therefore, alignment of the fibre coupling is relatively simple and stable and also robust against imperfect tracking.

Table 2 summarizes the specifications of the optical system (transmit and receive). These values are used in Sect. 2.4.3 to calculate the expected photon return rates.

2.2.4 Timing measurement and control

System-wide frequency and time synchronization is based on a Meinberg GPS-180 GNSS disciplined atomic clock, which provides a 10 MHz sine wave, a 1 PPS signal, and the datum over serial interface.

The timestamps are recorded using a Swabian instruments Time Tagger Ultra with a nominal timing precision of 9 ps. Additionally to the start, stop and PPS signals, laser trigger and detector gate are recorded as well on separate channels for debugging and monitoring.

Laser triggers and detector gate signals are generated by two Swabian Instruments Pulse Streamers. While one pulse generator runs a steady PPS-aligned 50 kHz trigger sequence for the laser, the other one produces a dynamically calculated gating sequence for the single photon detector, based on the expected time of flight to the target. Figure 4 shows the electronics installed in the cabinet.

Timing calibration is done roughly once per hour during regular operation. For this, the attenuated laser beam is guided directly towards the receiver aperture via a 45° mirror and a 45° diffuse surface. The nominal range to the calibration target is given by the distance from the mount axes intersection to the virtual intersection of the two 45° surfaces, and measured to 1.504 m.

2.2.5 Aircraft and laser safety

The output beam power is significantly above the maximum permissible exposure (MPE) defined in the laser safety norm EN 60825-1:2014. The miniSLR is thus classified as a class 4 laser system. While the beam expander reduces the power and energy density enough to avoid skin burns outside of the device, the limit for eye injuries is exceeded by about a factor of 200 at the exit aperture. Assuming a diffraction-limited beam divergence of about 50 µrad, the laser beam becomes eye-safe at a distance of about 10 km.

Laser emission is automatically shut off by the attenuator and safety shutter, unless a "clear" signal is given from the following checks (conducted by a special module in the control software):

Fig. 4 The inside of the cabinet houses the complete electronics for the system. Left rack top to bottom: Laser controller, PC, mount controller. Right rack: internet router, trigger and gate controller (Swabian Instruments), atomic clock (Meinberg), event timer (Swabian Instruments), network switch and two 12 V power supplies

- Pointing must be above the azimuth-dependent minimum elevation, which mirrors the adjacent buildings and obstacles. Below the elevation mask, the safety shutter can be opened, but only if the eye-safe attenuation is activated. This is mainly used for time calibration.
- Telescope must be tracking a target, not slewing or idling. The target must be whitelisted for laser ranging.
- No aircraft must be within 20° of the beam, within a distance of up to 20 km. Aircraft positions are received by a data stream from the German Air Traffic Authorities. For cross-check, a local ADS-B receiver (Jetvision Radarcape) and a thermal infrared camera (FLIR Tau-2, item 19) are installed.
- Operation status code must be nominal for a number of critical components, such as shutter and attenuator. Telescope pointing information must be up to date.

To ensure workplace safety, warning lamps, emergency stop button, access control and laser hazard signs are installed.

2.2.6 Slow control

To facilitate remote operation and simple trouble shooting, most power lines can be switched independently by software. This can be used e.g. to remotely restart components that are not working nominally. Programmable USB Hubs (Acroname 3P) are used to connect devices to the PC, which allow detailed monitoring of each USB port (data, power) and power-cycling USB-powered devices by software.

Temperature, humidity and air pressure are continuously recorded inside and outside of the device for monitoring, safety and SLR data evaluation.

2.3 Software

To operate the miniSLR, the control software orbital objects observation software (OOOS), developed at the institute for the previous laser ranging station "Uhlandshöhe", has been refined and improved. It is written almost entirely in python to facilitate rapid development and easy debugging. Exploiting multiprocessing and fast computing libraries (e.g. numpy), the software can handle all control tasks in real-time on a standard Linux or Windows PC. Special focus has been put into designing a clear and tidy graphical user interface (GUI), thus enabling fast training of observers and efficient work. A number of automation functions take over most of the standard tasks; however, a complete "hands-off" operation has not yet been achieved for laser ranging.

A range of processing nodes (also called daemons) take over different blocks of control. The nodes are loosely coupled to each other over a TCP/IP protocol. The GUI acts as a central node, orchestrating the work of the daemon nodes and channelling all user interaction (input and output). The daemon nodes connect to an abstract hardware layer, which in turn implements the actual device interfaces based on current configuration settings. Thus, changes to the system's hardware can easily be incorporated into the software.

Figure 5 shows a screenshot of OOOS running during an actual SLR observation.

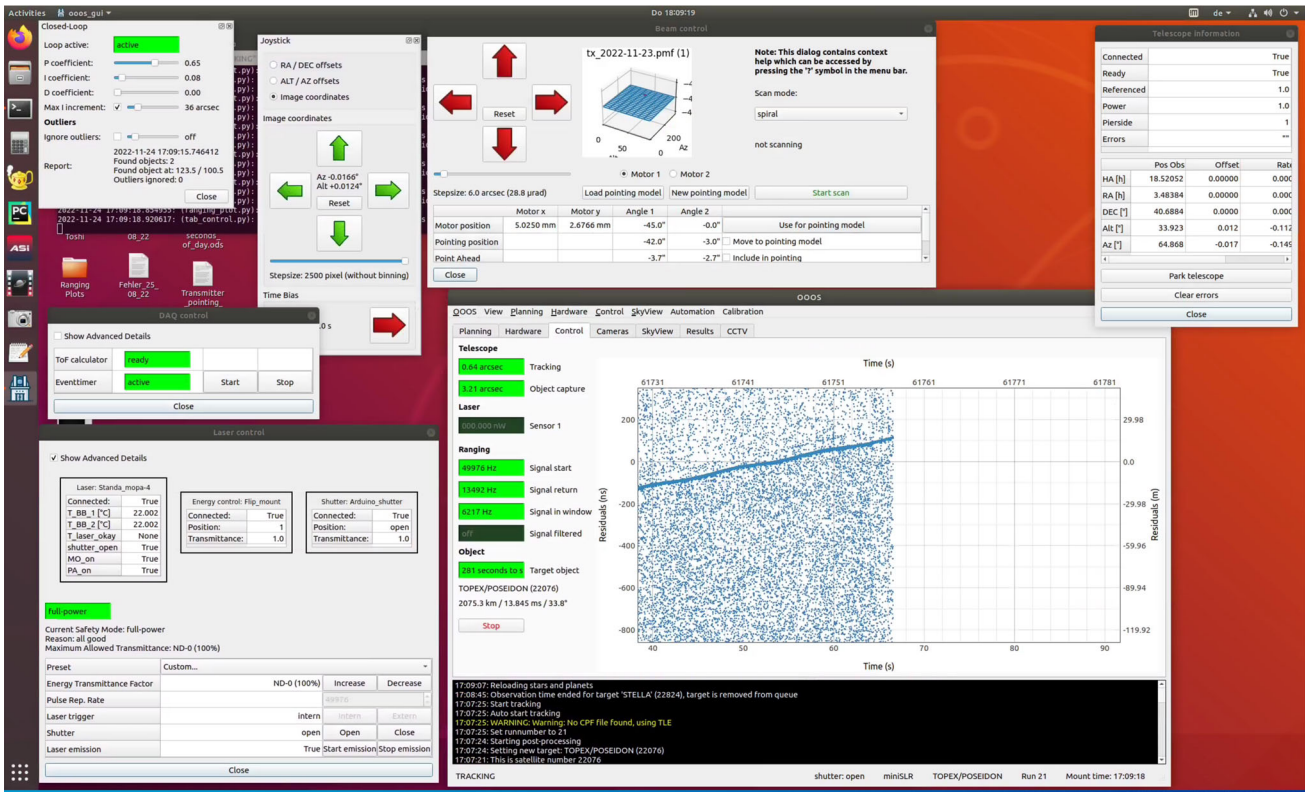

Fig. 5 Screenshot of OOOS during a ranging observation of satellite TOPEX

2.4 Expected performance

2.4.1 Single-shot precision

The timing uncertainty of a single range measurement ("single-shot precision") is given by the timing uncertainties of all contributing components:

$$\sigma_{\text{single}} = \sqrt{\sigma_{\text{L}}^2 + \sigma_{\text{D1}}^2 + \sigma_{\text{D2}}^2 + \sigma_{\text{ET}}^2 + \sigma_{\text{S}}^2} \tag{1}$$

with:

- σ_{L}, timing uncertainty due to the laser pulse duration
- σ_{D1}, time jitter of the start detector (photodiode)
- σ_{D2}, time jitter of receive detector (SPAD)
- σ_{ET}, time uncertainty of event timer
- σ_{S}, uncertainties caused by the design of the satellite retroreflectors. These are not subject to the miniSLR design and are therefore not considered here. For most satellites, the satellite signature is very small compared to the other contributing factors.

When evaluating Eq. 1, one has to observe that timing uncertainties are given by different metrics, the most common being full width half maximum (FWHM), root mean square (RMS), or standard deviation σ of a normal distribution. Assuming that all uncertainties are normal distributed (which is usually a reasonable approximation), it is possible to relate these quantities to each other with:

$$\sigma = 0.42 \times \text{FWHM} \tag{2}$$

$$\sigma \approx \text{RMS} \tag{3}$$

Using the specified values from the used components, an expected single-shot precision of 39 mm is derived (see Table 3).

2.4.2 Normal point precision

In post-processing, individual range measurements are averaged into normal points (NPTs). Recommended normal point durations are given by the ILRS and range from 5 to 300 s, depending on satellite altitude and expected return strength. Assuming a purely statistical error distribution, the precision of a normal point σ_{NPT} with N individual data points is given by

$$\sigma_{\text{NPT}} = \frac{\sigma_{\text{single}}}{\sqrt{N}} \tag{4}$$

Table 3 Timing uncertainty budget for the miniSLR components

Laser	210 ps	(Given as 500 ps FWHM)
Start detector	40 ps	
Receive detector	150 ps	(Worst case, probably better)
Event timer	9 ps	
Single-shot precision σ_{single}	261 ps	(Equivalent to 39 mm)

Single-shot precision is calculated using Eq. 1. All values are given as 1σ standard deviation

Given the single-shot precision of 39 mm, averaging about 1500 data points in a normal point should yield a normal point precision of 1 mm.

It must be pointed out that in reality the error distribution will not be purely statistical, but systematic errors also contribute. The main issue are drifts of timing delays (e.g. from photon detection to electrical signal), if they occur on the timescales of minutes. Drifts on longer timescales are eliminated by regular timing calibration. The amount of these contributions cannot be inferred from device specifications, but they are included in the experimental system validation (see Sect. 3.5).

2.4.3 Return rates

The system is designed to always operate in single photon mode, i.e. for each outgoing laser pulse the detector should see no more than one photon. This avoids any systematic time shifts in the receive detector due to multiple photon signals. As the number of actual photons returning is following a Poisson distribution, this can be achieved by ensuring a mean return quota (received photons per outgoing pulse) of much less than one, ideally below 0.1.

On the other hand, the mean number of photons must not be too small in order to still produce a visible signal. The actual limit is hard to estimate and depends on background brightness and a number of system specifications. For the described miniSLR set-up, the night time limit is around 5×10^{-5} (equivalent to roughly 2.5 Hz return rate).

The expected return quotas for different targets, atmospheric conditions and measurement geometries can be calculated using the modified radar link equation from Degnan (1993). It gives the mean number of expected photoelectrons per laser pulse as

$$n_{\text{pe}} = \left(E_{\text{T}} \frac{\lambda}{hc}\right) G_{\text{t}}\, \sigma_{\text{ocs}} \left(\frac{1}{4\pi R^2}\right)^2 A_{\text{r}}\, T_a^2\, \eta_{\text{t}}\, \eta_{\text{r}}\, \eta_{\text{d}} \qquad (5)$$

with:

- E_{T}, laser pulse energy
- λ, laser wavelength
- G_{t}, gain, a function of beam divergence and pointing stability
- σ_{ocs}, optical cross section of satellite reflector
- $\left(\frac{1}{4\pi R^2}\right)^2$, attenuation at distance R
- A_{r}, aperture of receive telescope
- T_{a}^2, atmospheric transmission
- η_{t}, efficiency of transmitter optics
- η_{r}, efficiency of receiver optics
- η_{d}, efficiency of detector

As some of the factors in Eq. 5 can only be estimated (e.g. beam pointing stability) or are subject to frequent changes (e.g. atmospheric conditions), the resulting numbers can be indicative only. A model based on this equation, but including elevation-dependent atmospheric effects, has been developed and experimentally verified by Meyer (2022). Using this model and the miniSLR specifications from Table 2, expected return quotas for a few important satellites have been estimated (see Table 4).

The numbers rapidly decrease with satellite altitude, owing to the R^4 factor in the link budget. While a very strong signal is expected from most LEO satellites, high satellites (especially Galileo) seem to be quite challenging. For low satellites, the return quota may even exceed the desired single photon maximum of 10%, if indeed these theoretical values can be achieved. In this case, the beam steering could be used to slightly misalign the beam, to reduce the return quota.

It should be pointed out that the optical cross sections used here are lower than theoretical values from Arnold (2003). Also, some of the miniSLR specifications are rather cautious, e.g. the receiver efficiency of 10%. It is thus conceivable that higher return rates than calculated here are possible in reality, especially under favourable atmospheric conditions.

In Sect. 3.3, some experimentally measured return rates are compared with the values estimated here.

3 Validation results and discussion

3.1 Data census and processing

The results presented here are based on observations made between November 2022 and April 2023.

Figures 6, 7, 8 show some typical examples of measurements taken. Most satellites in LEO and the two Lageos

Table 4 Satellite optical cross sections, return quotas and number of returns per normal point (NPT) expected for different satellites, based on the model referenced in Sect. 2.4.3

Satellite	NPT duration	Optical cross section	Return quota (%)	Returns / NPT
Grace-FO	5 s	0.6×10^6 m^2	70	175,000
Ajisai	30 s	6.1×10^6 m^2	18	270,000
Stella	30 s	0.1×10^6 m^2	3.7	55,000
Lares	30 s	0.28×10^6 m^2	1	15,000
Lageos	120 s	1.24×10^6 m^2	0.02	1200
Etalon	300 s	23×10^6 m^2	0.004	600
Galileo	300 s	3.1×10^6 m^2	0.0003	45

satellites can be tracked reliably, even in non-perfect conditions (light haze, scattered clouds). Higher satellites like Etalon, Glonass and Galileo have been tracked occasionally, but usually do not produce enough returns.

Post-processing of the data is done manually using OOOS. Data filtering and normal point generation are implemented according to the algorithm developed by the ILRS (Sinclair (2012)). A rejection interval of 2.5 times the RMS is used, as recommended for single photon systems. The normal points are indicated by red crosses in the plot. Summary measurement reports are generated in CRD (consolidated ranging data) format and used for further analysis.

3.2 Tracking accuracy

Accurate satellite tracking is fundamental to a productive SLR operation, but at the same time challenging for a relatively small mount. To allow for blind tracking (without visual acquisition), the tracking accuracy should be not much worse than the laser beam divergence of 10 arcsec ($\approx 50\,\mu$rad).

For the generation of pointing models, about 50–70 stars are recorded automatically. The process is slightly complicated by the fact that the mount cannot move the full 360° in azimuth, and has to use both pier sides (i.e. elevations above 90°) to cover the full sky. For each star, the offset from the camera target point is recorded. All offsets are subsequently fitted by an analytical model adapted from Wallace (2016).

With this, a pointing accuracy of better than 10 arcsec is achieved both on stars as well as on satellites with accurate predictions, including fast LEO satellites. Ranging with blind tracking has been shown successfully in a number of cases. Unfortunately, the pointing accuracy quickly deteriorates, and blind tracking usually becomes impossible after a few weeks. The reason for this is not yet determined, but it may be due either to instability in the mounting (on a gravel bed on the roof of a six-storey building), or some thermal effects in the mechanical mountings of the optical system. In order to keep a reasonably good tracking accuracy, the pointing model was updated every few weeks.

For the current study, most passes have been recorded at night, with visual guidance. Closed-loop tracking is performed automatically by the software if the target is visible. A few passes have been recorded with blind tracking or partial blind tracking (visual acquisition before entering the earth shadow).

Daylight tracking has been attempted once, but without success. Detector rates, however, seemed to be at a manageable level. Calibration records could be recorded without issues. The failure to see satellite returns is believed to be due to insufficient pointing accuracy.

Improving the pointing stability will be an important task in the further development of the miniSLR, to enable blind tracking at day and night.

3.3 Return rates

Figure 9 shows measured return numbers per normal point for some satellites. By and large, the measured numbers correspond roughly with the theoretical expectations from Sect. 2.4.3 (blue crosses). As expected from the modelling, large spreads between high and low data yields exist. These can be attributed to differences in tracking geometry, elevation angle, atmospheric transmission (local thin clouds) and changes in tracking accuracy.

Except for Lageos, the experimental values are somewhat lower than the calculated values, which are already at the low end of theoretical expectations. This may indicate that system losses are higher than assumed, and higher return rates may be achieved e.g. by better alignment of the optics.

3.4 Precision

During the post-processing, the single-shot RMS is calculated for each normal point. In calibration runs, the values are typically between 210 ps and 230 ps. In satellite tracks, the RMS depends slightly on the strength of the signal, probably due to imperfections in the data filtering. Figure 10 shows the normal point RMS values for a selection of satellites. Median values range from 220 to 330 ps. This is well compatible with the theoretical expectation of 261 ps / 39 mm (see Sect. 2.4.1).

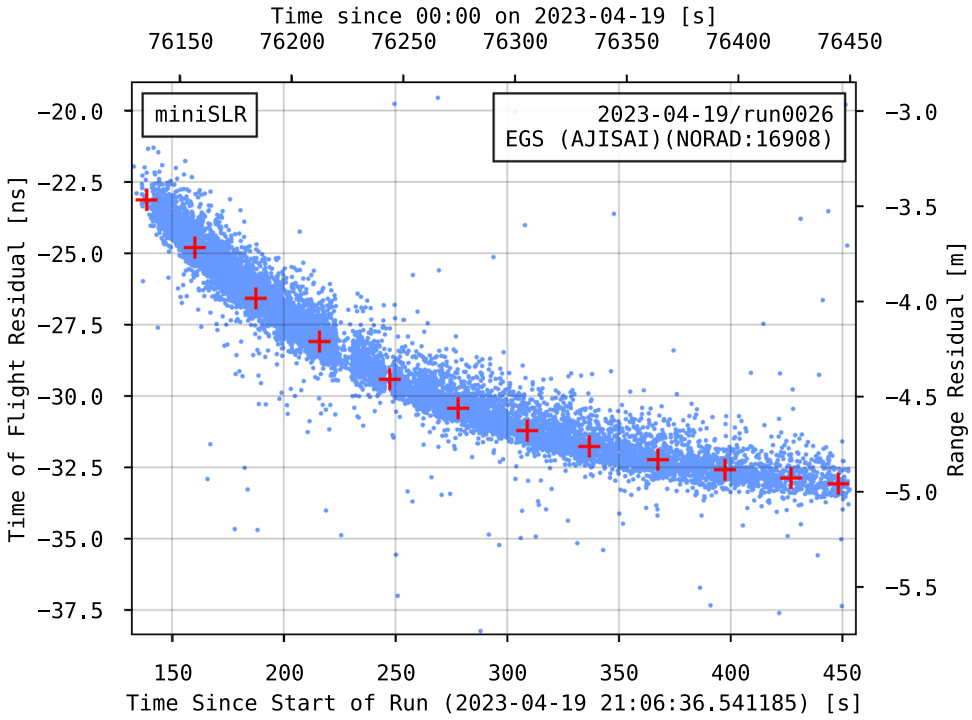

Fig. 6 Ranging plot of Ajisai. For clarity, only every 100th data point is shown. Normal points are marked in red. They contain between 40,000 and 200,000 individual ranges

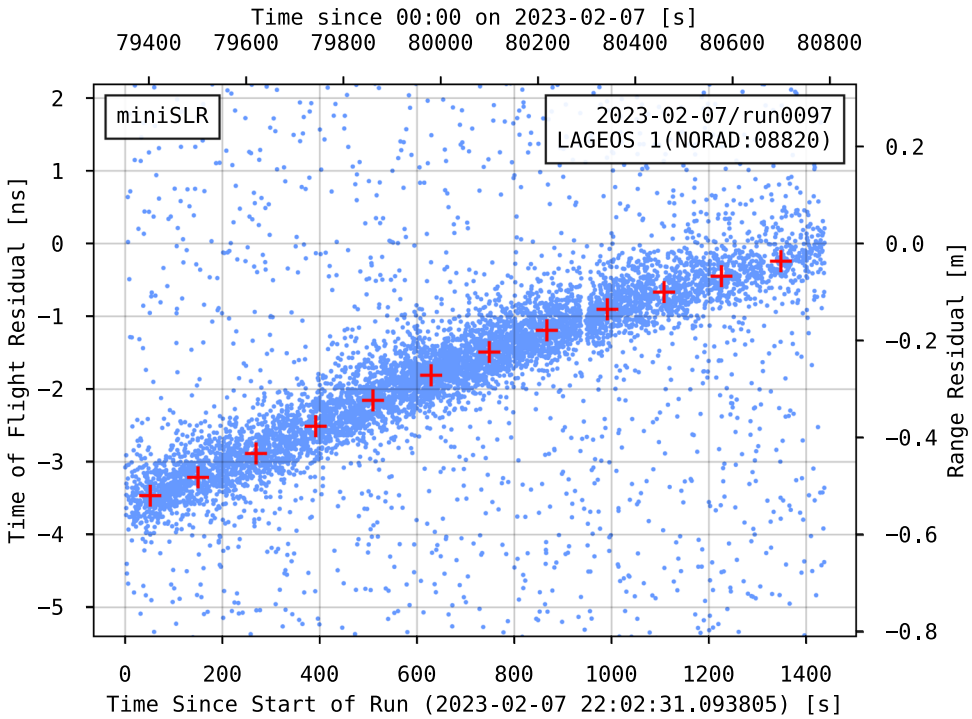

Fig. 7 Ranging plot of Lageos 1. For clarity, only every 3rd data point is shown. Normal points contain about 2,000 ranges each

As can be seen from Fig. 9, the expected minimum of 1,500 data points per normal point is often achieved. For some Lageos points, and usually for high satellites (such as Etalon-2, shown in Fig. 8), it can be lower.

A quality cut has been applied at 300, i.e. NPTs with less than 300 data points are discarded. Such low data normal points may occur at e.g. beginning or end of measurements, during interruptions due to aircraft warnings, from imperfect tracking, or scattered clouds. Ideally, one would like to increase the quality cut to 1500 points, to achieve the envisaged averaging effect (see Sect. 2.4.2); however, this would have eliminated too much data in the present study. With a higher quality cut, a slightly improved normal point precision may be achieved.

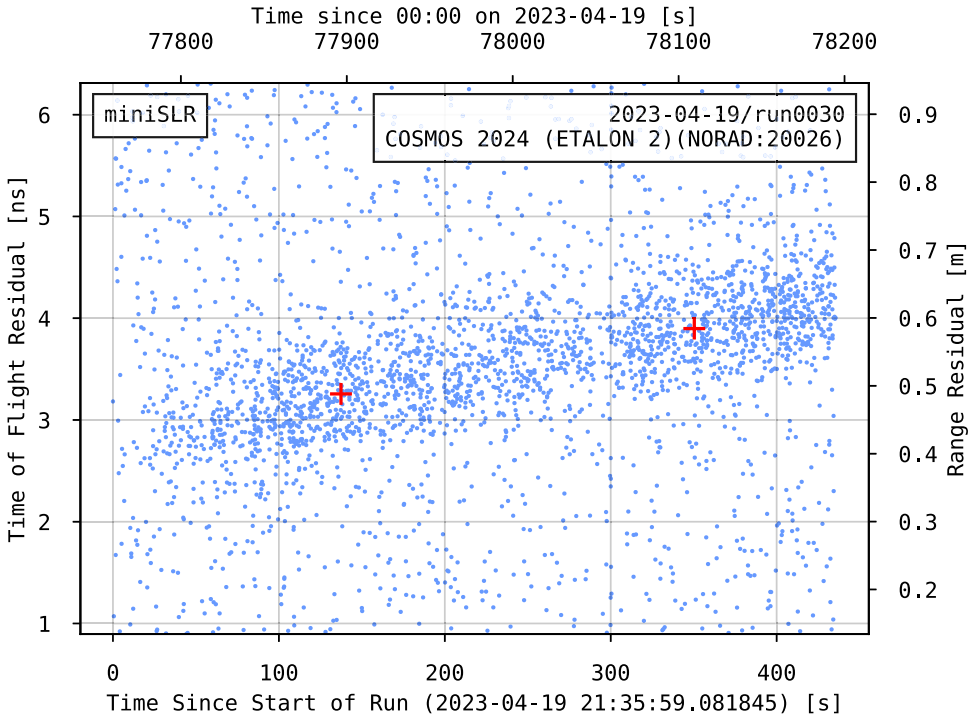

Fig. 8 Ranging plot of Etalon 2. Normal points contain around 800 ranges each

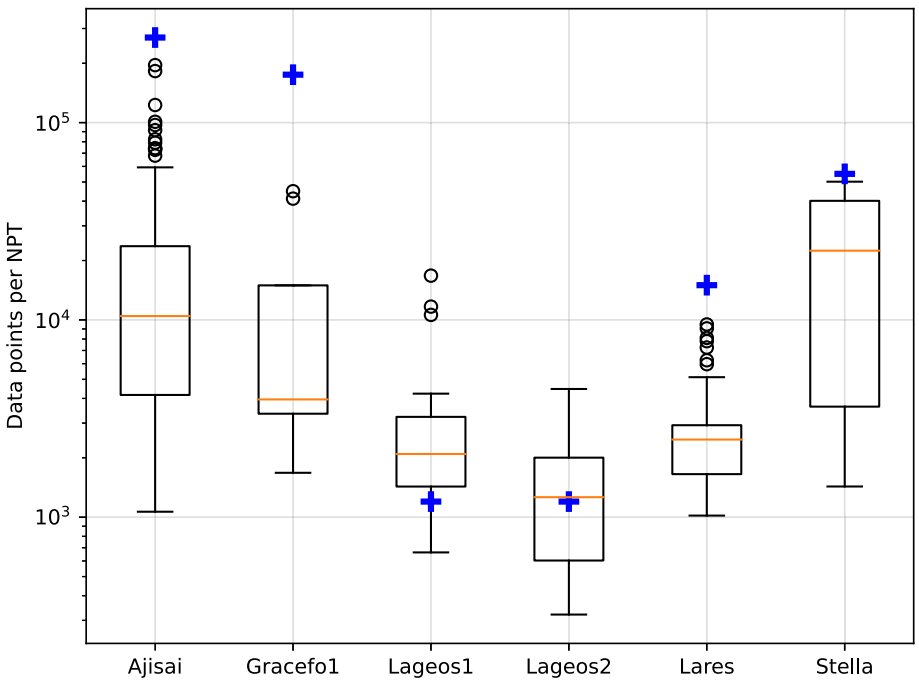

Fig. 9 Measured return rates, given in data points per normal point (NPT). Normal point durations are 5 s for Grace-FO, 30 s for Ajisai, Lares and Stella, and 120 s for the Lageos satellites. The boxes show the range from first to third quartile of the return numbers, the horizontal line denotes the median. Outliers beyond twice the inter-quartile range are shown as individual circles. Blue crosses mark the theoretical expectation from Table 4

3.5 Accuracy

To obtain a realistic estimation of the system performance, the data has kindly been analysed by Toshimichi Otsubo from Hitotsubashi University, using his rapid quality control software (Otsubo et al. 2019). It generates global fits for the orbits of all considered satellites, based on data from all SLR stations that have uploaded measurements for the time period in question. Thus, the analysis provides a measure of one station's accuracy, relative to all other stations in the network.

The most relevant results of this analysis are:

- Station coordinates
- Station range bias (adjusted once for each station)
- Pass range bias (adjusted for every pass)
- Normal point precision, estimated from scatter of normal points around fit.

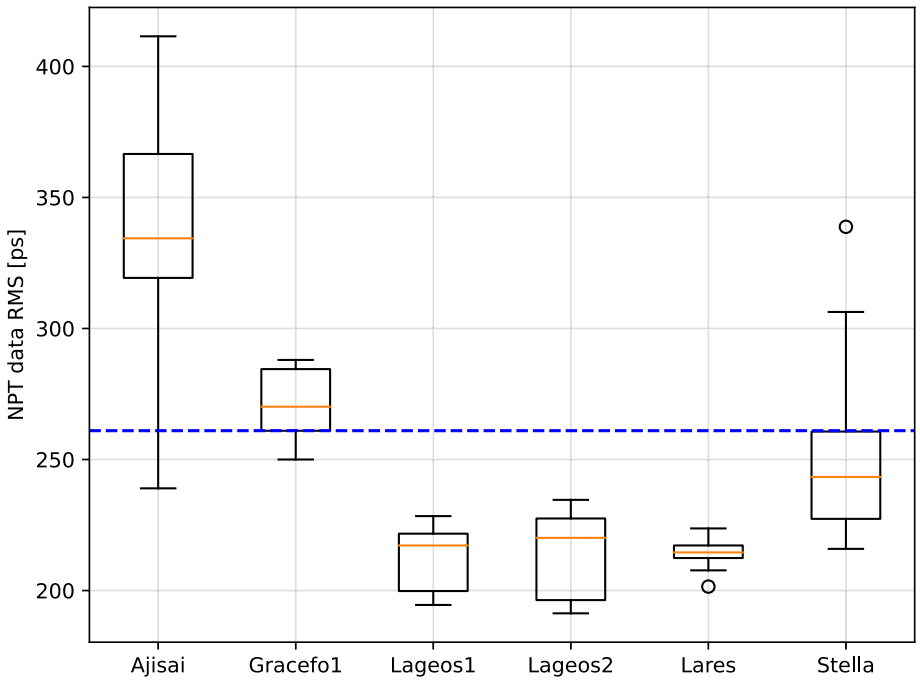

Fig. 10 Measured RMS of data within a normal point (NPT). The theoretical expectation for this value is given as 261 ps (blue dashed line, see Table 3). See caption of Fig. 9 for further explanation

Table 5 Station coordinates in ITRF2014, as measured by a local surveyor, and by SLR data from February 2023

Coordinate	Local survey	SLR analysis
x	4,160,755.242 m	4,160,755.135 m
y	666,638.631 m	666,638.658 m
z	4,772,593.195 m	4,772,593.327 m

For the analysis of the miniSLR accuracy, only data taken during 5 nights from February 7 to 13, 2023, is considered. Five satellites are included in the analysis: Lageos 1 and 2, Ajisai, Stella and Lares. The data comprise 15 passes with a total of 163 normal points of these satellites. Based on this limited dataset, a first estimation of the experimental performance of the system is performed.

Coordinates of the station invariant point (intersection of the two mount axes) have been measured by a surveyor in a local datum, and transformed to ITRF2014 Cartesian coordinates. They agree to the coordinates from SLR data to within 20 cm (see Table 5). The reason for this rather large deviation may be inaccuracies in the conversion of the local datum into ITRF2014, or insufficient SLR data for a very accurate position estimate.

The station range bias is fitted with 3.4 cm. While already encouragingly small, this number is still larger than expected from system specifications. Possible reasons could be a wrongly measured distance to the local calibration target, or systematic biases between calibration and actual satellite measurements (e.g. by the attenuator).

The pass-by-pass variation of the range bias is found to have an RMS of 7.4 mm. This can be compared to the pass range bias RMS of the other stations that have supplied data in the same timespan for the same satellites (see Fig. 11). While the best stations in the network, like Graz, Yarragadee or Wettzell, achieve values below 3 mm, other station are at the same order of magnitude as the Stuttgart miniSLR, or worse.

The normal point precision, i.e. the scatter of normal points around the fitted (and bias-corrected) orbits, averages to 4 mm. Again, the comparison with other station shows that the miniSLR achieves a satisfactory performance (Fig. 12).

Please note that Figs. 11 and 12 show only stations that have supplied data for the same period of time. Hence, some operational ILRS stations are missing (e.g. Matera, Shanghai, Simosato, etc.). The performance of all ILRS stations can be viewed in ILRS (2023). The numbers there are in the same order of magnitude as the numbers shown here for the limited dataset.

While the low number of data points limits the statistical significance of these results, they are a good indication of the possible performance of the system. It seems fair to claim that the miniSLR can indeed reach a similar accuracy as conventional stations, and thus be valuable tool for geodesy and other SLR applications. Long-term stability and more statistical significance of the results will require more data, which will be collected and supplied to the ILRS in the future.

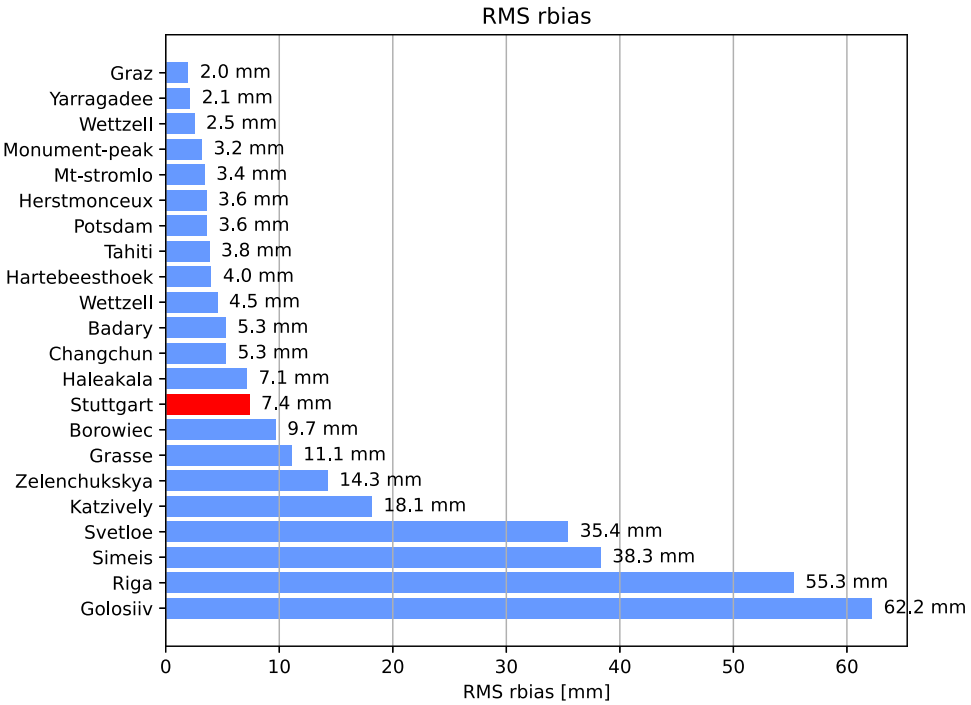

Fig. 11 RMS of pass range biases according to data analysis described in Sect. 3.5. It displays the changes in the pass-to-pass range bias offsets applied to match the global orbital fits

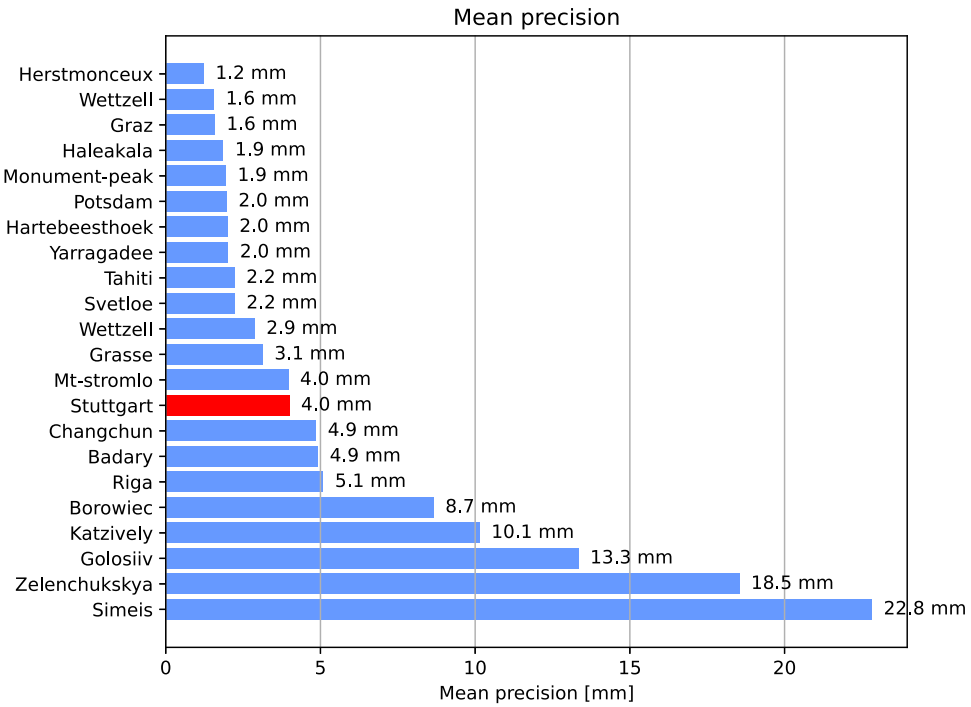

Fig. 12 Mean precision according to data analysis described in Sect. 3.5. The mean precision is given as scatter of normal points around the fitted orbit, after application of a constant range bias, and a pass-dependent range and time bias

4 Conclusion and outlook

4.1 Results

In the scope of the work described here, a fully functional prototype of a minimal SLR system has been constructed, commissioned and tested. The validation was done on existing ILRS supported satellites at all relevant altitudes and with different retroreflector configurations. The results indicate that ranging to most relevant targets can be performed with an accuracy comparable to existing, conventional SLR systems. Success rates and productivity (passes per hour) are similar to standard stations as well.

Remote operation is possible and has been conducted regularly for data taking. However, maintenance tasks and adjustments still frequently require on-site presence of a qual-

ified engineer. To enable future fully remote operation, the failures and instabilities must be analysed and eliminated as far as possible. Nevertheless, in mid-term perspective, the system will likely continue to require on-site presence of qualified technical staff, for on-demand works.

Compared to state-of-the-art SLR systems, the miniSLR currently still lacks the possibility to consistently range to GNSS satellites, and to reliably perform blind ranging (without visual acquisition). Also, daylight ranging has not yet been demonstrated.

4.2 Possible improvements

The issues with blind tracking can probably be solved with a more rigid mechanical construction of the optical bench, or even just with a more suitable operating location. Presumably, this would also enable daylight ranging. While the effect of such improvements is yet to be shown, the problems seem not to be immanent to the minimal SLR concept.

The issue of ranging to GNSS targets, on the other hand, is indeed connected to the small size of the receiver aperture. Both theoretical estimates and experimental results seem to indicate that despite the rather high laser power of 5 W, not enough photons are received to reliably detect returns from these satellites. Since ranging to GNSS targets is an important SLR application, future developments will attempt to improve the return rates further, e.g. by:

- Increasing the exit aperture, thus decreasing the divergence (possibly coupled with a motorized divergence control)
- Improving the transmission in the receive path by better alignment and a better spectral filter.
- Using a single photon detector with a slightly higher detection efficiency, e.g. an MPD-PDM-IR MPD (2020), and using free-space mounting rather than fibre coupling.

Increasing the laser power or the telescope aperture (slightly) may also be considered, but are not favoured due to the significant impact on the overall system design.

4.3 Applications and impact

The current version of the miniSLR seems mainly suitable for the following applications:

- Geodetic measurements, especially at remote locations currently not well covered by the existing SLR network
- Supporting high-performance stations, relieving them of some of the daily tracking load
- Mission support for LEO satellites
- Conjunction assessment, if at least one object is equipped with retroreflector
- Studies and experiments requiring a flexible SLR ground station

If a future version can deliver stable ranging to GNSS targets, it can also be used as a ground station for any GNSS constellation. This could result in a major relief of other stations, since GNSS targets take up by far the most observation time.

From first estimations, it is believed that the end user price for a new miniSLR station can be around a factor of 3–5 lower than for a simple standard SLR station, and about a factor of 10 lower than for a high-end multipurpose optical ground station. Combined with the reduced infrastructure and space requirements, this may trigger the use of SLR systems in locations and applications in which it was previously not feasible. For users operating on a tight budget (e.g. institutions in the Global South, or commercial operators), the miniSLR may be a door-opener to SLR. Conversely, at a given budget it now becomes possible to install several miniSLR systems rather than one high-end SLR station. Depending on the use case, the impact on the data products of such a small, well-distributed network may be better than of one high-end station.

4.4 Further developments

The Stuttgart miniSLR will continue to deliver data to the ILRS for further validation. As part of a research project, it will also be equipped with polarization optics to test the feasibility of satellite identification through polarizing retroreflectors (Bartels et al. 2022). Additionally, it will be used to participate in laser ranging research projects.

In parallel, a commercial version of the miniSLR will be designed and constructed by DiGOS Potsdam GmbH. The current shortcomings of the first prototype will be addressed and hopefully be mitigated. In particular, it is planned to achieve:

- Consistent blind tracking due to a better mount and improved mechanical stability
- Daylight ranging based on improved tracking
- GNSS ranging due to an improved optical system, e.g. larger transmit aperture for smaller divergence, motorized divergence control and improved optical components for better transmission in the receive path.

First results from this new DiGOS miniSLR prototype are expected in 2025.

Supplementary information

The miniSLR design is partly patented. The name "miniSLR" is a registered trademark.

Acknowledgements The authors would like to acknowledge contributions to this project by former team member Ewan Schafer, former team member Paul Wagner, Robin Neumann and Luis Gentner, who supported the construction and data taking, the institute's mechanical, electronic and IT department for their continued effort in supporting this project, Prof. Toshimichi Otsubo from Hitotsubashi University, Tokyo, for his continued support and encouragement.

Author Contributions DH co-developed the concept of the miniSLR, lead the technical development and wrote the paper. FN worked on the technical implementation of the miniSLR and conducted measurements. TM conducted measurements, calculated theoretical return rates and supported the software development. WR co-developed the concept and vision of the miniSLR and had the administrative lead of the project.

Funding Open Access funding enabled and organized by Projekt DEAL. The work described here was mainly funded by DLR as part of a technology transfer project.

Availability of data and materials The normal point data generated and analysed for this paper are available on the EDC website (EDC (2023)). Raw data are available from the corresponding author on reasonable request.

Code Availability The code used to process and analyse the data is part of the software package OOOS, which is licensed under GPLv3. It is available from the corresponding author on reasonable request.

Declarations

Conflict of interest DH declares that he is involved in the commercial distribution of the miniSLR at DiGOS Potsdam GmbH and may profit from sales of the system.

References

Arnold D (2003) Cross section of ilrs satellites. https://ilrs.gsfc.nasa.gov/docs/CrossSectionReport.pdf

Bartels N, Allenspacher P, Hampf D et al (2022) Space object identification via polarimetric satellite laser ranging. Commun Eng 1:5

Courde C, Torre J-M, Samain E et al (2017) Satellite and lunar laser ranging in infrared. In: Proceedings SPIE 10229, photon counting applications, 102290K

Degnan JJ (1993) Millimeter accuracy satellite laser ranging: a review. Contrib Space Geod Geodyn Technol 25:133–162

Eckl JJ, Schreiber U, Schüler T (2017) Satellite laser ranging in the near-infrared regime. In: Proceedings SPIE 10229, photon counting applications 102290J

EDC Website (2023) https://edc.dgfi.tum.de/en/

Glaser S, König R, Neumayer K et al (2019) Future SLR station networks in the framework of simulated multi-technique terrestrial reference frames. J Geod 93:2275–2291

Hampf D, Schafer E, Sproll F et al (2019) Satellite laser ranging at 100 kHz pulse repetition rate. CEAS Space J 11:363–370

Hampf D, Riede W, Bartels N et al (2021) A path towards low-cost, high-accuracy orbital object monitoring. https://conference.sdo.esoc.esa.int/proceedings/sdc8/paper/251/SDC8-paper251.pdf

ILRS (2023) Global performance report cards. https://ilrs.gsfc.nasa.gov/network/system_performance/global_report_cards/monthly/2023/02/2023_02_Monthly_report_card.html

ILRS Website (2023) https://ilrs.gsfc.nasa.gov/

Kehm A, Bloßfeld M, König P et al (2019) Future TRFs and GGOS: Where to put the next SLR station? Adv Geosci 50:17–25

Meyer T (2022) Analysis of the performance parameters of satellite laser ranging (slr) systems based on the link budget underexemplary inclusion of the minislr system. https://elib.dlr.de/192865/

MPD (2020) PDM-IR http://www.micro-photon-devices.com/MPD/media/Datasheet/PDM-IR%20Datasheet%20window.pdf

Nicolas J, Pierron F, Samain E et al (2001) Centimeter accuracy for the French transportable laser ranging station (FTLRS) through sub-system controls. Surv Geophys 22:449–464

Otsubo T, Matsuo K, Aoyama Y et al (2016) Effective expansion of satellite laser ranging network to improve global geodetic parameters. Earth Planet Sp 68:1–7

Otsubo T, Müller H, Pavlis E et al (2019) Rapid response quality control service for the laser ranging tracking network. J Geod 93:2335–2344

Pearlman M, Arnold D, Davis M et al (2019) Laser geodetic satellites: a high-accuracy scientific tool. J Geod 93:2181–2194

Pearlman M, Noll C, Pavlis E et al (2019) The ILRS: approaching 20 years and planning for the future. J Geod 93:2161–2180

Sinclair T (2012) Ilrs normal point algorithm. https://ilrs.gsfc.nasa.gov/data_and_products/data/npt/npt_algorithm.html

Völker U, Friedrich F, Buske I et al (2013) Laser based observation of space debris: Taking benefits from the fundamental wave. In: Proceedings 6th European conference on space debris. https://elib.dlr.de/86306/

Wallace P (2016) TPOINT: a telescope pointing analysis system

Wilkinson M, Schreiber U, Procházka I et al (2019) The next generation of satellite laser ranging systems. J Geod 93:2227–2247

Xue L, Li Z, Zhang L et al (2016) Satellite laser ranging using superconducting nanowire single-photon detectors at 1064 nm wavelength. Opt Lett 41(16):3848–3851